

Supplementary Material

Quantification of Lung Inflammation in Cystic Fibrosis during Respiratory Tract Exacerbation using Diffusion-Weighted Magnetic Resonance Imaging

Methods

This was a cross-sectional observational study of patients with cystic fibrosis (CF) with and without respiratory tract exacerbation (RTE). All subjects with RTE attended on a two occasions, whilst admitted for RTE (baseline) and after intravenous antibiotic therapy (follow-up), and underwent a series of clinical, lung function and radiological examinations during the same visit. Similarly, control subjects repeated the study protocol over the same median time gap as the RTE group. Visits took place between September 2011 – September 2013.

This study was approved by the Ca' Foncello Regional Hospital Ethics Committee, protocol n. 314/AULSS9. Parents/guardians signed informed consent and paediatric subjects provided assent.

Patient selection

Respiratory tract exacerbation group

No universally accepted definition of a respiratory tract exacerbation (RTE) exists. A general definition, described as “clinical need for additional treatment as indicated by acute changes in clinical parameters”, has been recently adopted by the Eurocare CF Working Group.¹ These acute changes during RTE include: change in sputum; increased cough; increased malaise; fatigue or lethargy; anorexia or weight loss; decrease in spirometry outcomes by 10% or more or radiographic changes; and increased dyspnea.

These changes are also used by the Rosenfeld criteria to score the clinically likelihood of RTE in patient with CF (Tab. S1)². All subjects enrolled in the study were scored with the Rosenfeld criteria for RTE both at baseline at follow-up in.

Table S1 Rosenfeld criteria for respiratory tract exacerbations

Rosenfeld Criteria	PEX scoring system
<ul style="list-style-type: none">• Reduced exercise tolerance• Increased cough• Increased sputum/cough congestion• School or work absenteeism• Increased adventitial sounds on lung examination• Reduced appetite• Reduced FEV₁ ($\geq 10\%$ predicted)	<ul style="list-style-type: none">• Each criterion is assigned a coefficient• PEX score is the sum of the coefficient per each criterion when present• Threshold value to define RTE is 2.6

PEX=pulmonary exacerbation scoring system, RTE=respiratory tract exacerbation, FEV₁= Forced expiratory volume in 1 sec

29 **Clinically stable CF patients – Control group**

30 Clinically stable patients with CF were asked to participate to the study at the annual follow-up visit. Clinically
31 stability was defined when patient had no signs or symptoms of RTE in the previous 6 month to the visit. Each
32 control subject was selected after inclusion of an RTE group subject and matched for age, sex, and mean of FEV₁ in
33 the previous 6 months before the visit.

34

35 **Study protocol**

36 The study protocol consisted of clinical examination, spirometry and magnetic resonance imaging (MRI). Each RTE
37 subject performed the study protocol at admission (baseline) and after intravenous antibiotic treatment (follow-up).
38 Each control subject performed the study protocol twice with a similar median time gap (~ 20 days) of RTE
39 subjects.

40

41 **Clinical examination**

42 Clinical examination started with collection of recent patient history, in particular variation on coughing, amount
43 and color of sputum, dyspnea, exercise tolerance, and work or school absenteeism. Physical exam consisted of heart
44 and respiratory rate measurements, O₂ saturation, weight and height recording for body mass index measurement,
45 oral and ear inspection, cardiac and lung auscultation. During the clinical examination, was also performed the PEX
46 score to define whether the subject with CF had or not RTE.

47

48 **Spirometry**

49 Repeated spirometry efforts were performed until 3 acceptable maximal maneuvers were obtained according to
50 “ATS/ERS guidelines” using a Masterscope (Jaeger-Carefusion, Hochberg, Germany) spirometer³. When
51 spirometry traces showed evidence of incomplete expiration, cough, and air leak were repeated. Acceptable
52 repeatability was obtained when the difference between the largest and next largest maneuvers was ≤ 100 ml or 5%
53 depending on which was the larger value. The recorded result for Forced expiratory volume in 1 second (FEV₁) and
54 forced vital capacity (FVC) was the highest achieved across all technically correct efforts, with the ratio calculated
55 from this FEV₁/FVC and reduction in forced expiratory flow at 25-75% of the FVC (FEF₂₅₋₇₅) were expressed as %
56 of predicted value.

57

58 **MRI**

59 MRI was performed at 1.5 Tesla (MAGNETOM Avanto, Siemens Healthcare, Erlangen, Germany) using
60 morphological and functional sequences.

61 Morphological sequences included axial and coronal end-expiratory triggered Periodically Rotated Overlapping
62 Parallel Lines with Enhanced Reconstruction (PROPELLER; SIEMENS brand name, BLADE) with proton density
63 (PD) weighting (TR/TE/alpha/TA: 710/26 ms/150°/4' 25'', voxel size 1 x 1 x 6 mm³; bandwidth 601 Hz/pixel, slice
64 gap 0 mm, average n=4)⁴, and breath-hold spirometry gated axial and coronal steady state free precession (SSFP;
65 SIEMENS brand name, TrueFISP) with T₂/T₁ weighting (TR/TE/alpha/TA: 229/0.99 ms/66°/14'', voxel size 2.3 x

66 2.3 x 6 mm³; bandwidth 1291 Hz/pixel, slice gap 0 mm, average n=1). For the breath-hold MRI acquisitions,
67 subjects were trained to obtain a maximal breath hold time of 15 seconds at ≥95% Total Lung capacity (TLC) and at
68 ≥ 90% residual volume (RV) using an MRI compatible spirometer (Software B3BOX, Biomedin, Padova, Italy).

69 The functional data were acquired in the axial plane using a diffusion-weighted (DW) single shot echo-planar
70 imaging (EPI) sequence prototype (TR/TE = 4800ms/54ms, voxel size 2.5 x 2.5 x 6 mm³; bandwidth 1644 Hz/pixel,
71 slice gap 1.8 mm, average n=3) with end-expiratory triggering. Eleven b-values at different time intervals (0, 10, 20,
72 30, 50, 70, 100, 150, 200, 400, 800 s/mm²) were acquired in three orthogonal directions. The entire MRI scan
73 required approximately 25-30 min.

74 **Image analysis**

75 Image analysis was conducted using the picture archiving and communication system (PACS) SYNAPSE (Fujifilm
76 Healthcare Europe, Dusseldorf, Germany). MRI images were anonymized and evaluated in random order by two
77 radiologists (V.T. and S.B.), with 4 and 8 years of experience in thoracic MRI scoring respectively. Both
78 radiologists were blinded to any clinical information and to each other's MRI assessment.

80 **Morphological scoring system: CF-MRI scoring system**

81 Morphological images BLADE and TrueFISP were scored with the Cystic Fibrosis MRI scoring system (CF-MRI),
82 a scoring system derived from the Brody scoring system and adapted to MRI^{4,5}. This scoring system evaluates the
83 five lung lobes and lingula as the sixth lobe. The CF-MRI scores assess the following components: bronchiectasis,
84 mucus plug, parenchymal changes (atelectasis, consolidation, ground-glass), trapped air. Differently from CT, air
85 wall thickening is combined with bronchiectasis in the CF-MRI, because of the lower spatial resolution of MRI⁴. For
86 the same reason, the pattern of trapped air is not scored in CF-MRI, as this has previously been shown to be
87 unreliable⁴. A composite score for each component is calculated and expressed as a percentage of a maximum score,
88 on a 0–100 scale. The higher the score the more severe the disease.

90 **Diffusion Weighted Magnetic Resonance Imaging (DW-MRI) Analysis**

92 **DW images and Apparent Diffusion Coefficient (ADC) maps: qualitative and quantitative analysis**

93 DW-MRI measures the random Brownian motion of the extra-cellular water molecules in the body. In biologic
94 tissues, this motion is dependent and limited by interactions with cell membranes and macromolecules. In dense
95 cellular tissues or in case of cellular swelling this water motion is reduced or “restricted”, because of reduced
96 extracellular space and by cell membranes. Tumors, edema and inflammation are all characterized by restricted
97 diffusion.

98 DW-MRI provides two types of images: the native DW images, which are repeated at least twice, varying a
99 parameter in the sequence called “b value”, and the post-processed Apparent Diffusion Coefficient (ADC) map.

100

101 The sensitivity of the DW-MRI technique to water motion depends on scanner's parameters, which are summarized
102 by the b-value, expressed as sec/mm^2 ^{6,7}. Water molecules with a large degree of motion (i.e. fluid) will have a fast
103 DWI signal decay with high b-values ($>700 \text{ s}/\text{mm}^2$). Conversely, slow-moving water molecules show a lower DWI
104 signal decay with large b-values. DW-MRI is typically performed using at least two b values to enable meaningful
105 interpretation⁸. The interpretation of the relative attenuation of DWI signal intensity on images obtained at different
106 b values, allows the analysis of different tissue components. For instance, in a tumor with cystic and solid
107 components, the cystic portion will show greater signal decay on high b-value images because water diffusion is less
108 restricted. By contrast, the more cellular solid portion will show relatively high signal intensity at high b-value⁸.
109 Therefore, in case of tumors and inflammation high DWI signal (bright) can be visually assessed at high b-values.
110 However, this qualitative visual assessment is limited by the T2 shine-through artefact, where tissues with long T2-
111 relaxation time have high DWI signal at high b-value, despite normal water diffusion⁷. This potential source of error
112 can be eliminated by using an apparent diffusion coefficient ADC map, which is an average image obtained by DWI
113 signal at different b-values. Areas of restricted diffusion in highly cellular tissue have low ADC values compared
114 with less cellular areas that return higher ADC values. It is important to notice that areas of restricted diffusion will
115 appear as low-signal intensity areas (dark) on ADC map, and as high-signal intensity areas (bright,) on DW images
116 (opposite to ADC maps). Hence, ADC maps are complementary to DW images for a correct interpretation of DWI
117 signal.

118
119 In this study, we combined a semi-quantitative scoring system to score DW-MR images and quantitative
120 measurement performed on ADC maps. The DWI scoring system presented in table S2 describes how the lesions
121 with high-signal intensity on DW-MR images with high b value, defined as hotspots, were quantified. This method
122 proved to be reliable in previous studies, with high sensitivity and specificity⁹⁻¹². A minimum of two b-values
123 should be used to assess mono-compartmental diffusion analysis, such as $0-800 \text{ s}/\text{mm}^2$ ⁸. More sophisticated analysis
124 (bi-compartmental) can be obtained by using Intravoxel incoherent motion analysis (IVIM), which requires a higher
125 b-values sampling between $0-200 \text{ s}/\text{mm}^2$ (i.e. $0-25-50-100-150-200 \text{ s}/\text{mm}^2$) and larger steps after $200 \text{ s}/\text{mm}^2$ (i.e.
126 $200-400-600-800-1000$)^{13,14}. In this study, we did not perform IVIM analysis, because DW-MRI data needed image
127 registration post-processing for reliably performing IVIM technique. At the time of the study, we did not have
128 dedicated software for imaging registration.

129

130 **Table S2 – DW-MRI analysis**

Parameter	Score
Presence of hotspot	<ul style="list-style-type: none"> • Score 1: presence of hotspots greater than 5% of lobe volume • Score 0: no hotspot
Extension	<ul style="list-style-type: none"> • Score 1: hotspots occupying a volume smaller than 33% of the lobe • Score 2= hotspots occupying a volume between 33% and 67% of the lobe • Score 3: hotspots occupying a volume greater than 67% of the lobe
Signal Intensity (SI) dominant hotspot	<ul style="list-style-type: none"> • Score 1: SI hotspots greater than SI cord spine • Score 0: SI hotspots smaller than SI cord spine
Mean signal intensity (SI_{mean})	<ul style="list-style-type: none"> • Score 1: mean SI hotspots within a lobe is greater than SI of cord spine • Score 0: mean SI hotspots within a lobe is smaller than SI of cord spine
Sub-score A	<ul style="list-style-type: none"> • $A = (E + SI)$
Sub-score B	<ul style="list-style-type: none"> • $B = (E + SI_{mean})$
Total DWI score (DWI)	<ul style="list-style-type: none"> • $DWI = P+A+B$

131 DW images were scored using a semi-quantitative scoring system which assesses each lobe using the following
 132 parameters: presence of hotspot (P), extension of hotspot (E), signal intensity of the dominant hotspot (SI) and
 133 average signal intensity of the hotspots within a lobe (SI_{mean}). For each lobe, we obtained two sub-scores: A = (E +
 134 SI) and B = (E + SI_{mean}). The total DWI score is the sum of P + A + B, and the maximum possible score is 54. The
 135 DW images with the highest b-value (b= 800 s/mm²) were scored.

136 ADC map were used to objectively quantify diffusion in those dominant pulmonary lesions, which showed restricted
 137 diffusion at high b-values¹⁵. The ADC maps were generated automatically from each DW image by the MR system
 138 software using all b-values (Syngo software version VB19, SIEMENS, Erlangen, Germany).

139 A region-of-interest (ROI) was positioned in these dominant lesions with restricted diffusion on ADC maps, using a
 140 freehand tracing tool, at baseline and follow-up MR examination. A dominant lesion was defined according two
 141 criteria: size, (the largest lesion within a lobe,) and signal intensity (SI) (the lesion with DWI SI higher than the
 142 spine at b=800 s/mm²). Adjacent vessels and areas with susceptibility artifact caused by air-tissue interface were
 143 excluded from image analysis. ROI covering the entire size of the hotspot was placed in the same location on ADC

144 maps from MRI at baseline and follow-up in both groups. When the hotspot was not visible in the follow-up
145 examination, the same ROI size and location of the baseline examination was kept to compute ADC. When no
146 hotspots were identified (i.e. control group), three ROIs of 100 mm² were randomly positioned in the lung
147 parenchyma and the mean value was used as ADC value for that subject.

148 **Results**

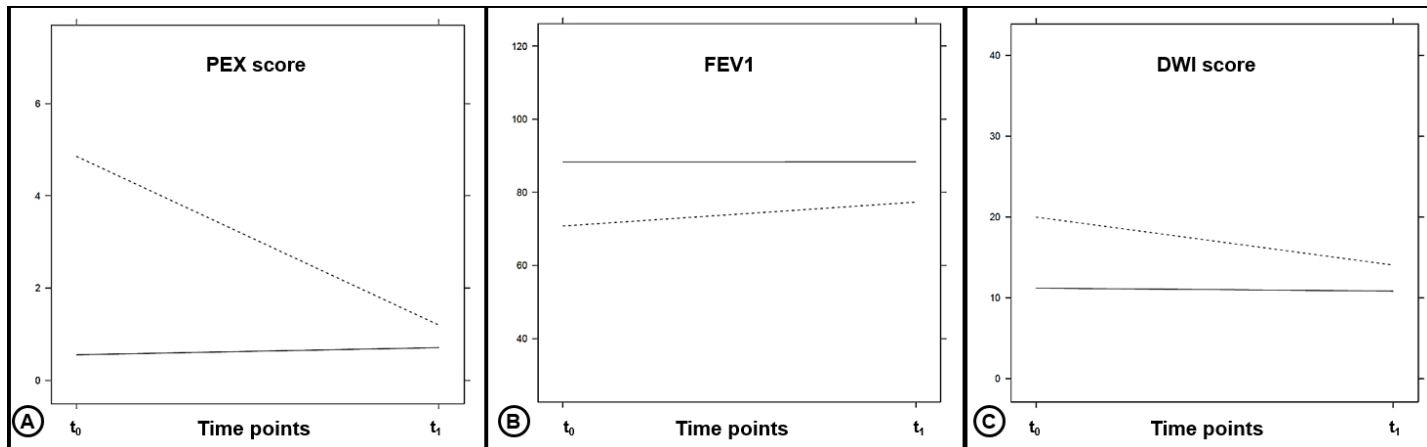
149 **Score reliability**

150 **Table S3 Inter and intra-observer agreement for DWI score at baseline and follow-up MRI**

Score	Inter-observer agreement		Intra-observer agreement	
	ICC baseline MRI	ICC follow-up MRI	ICC baseline MRI	ICC follow-up MRI
Sub-score A	0.918	0.904	0.947	0.920
Sub-score B	0.895	0.873	0.936	0.894
Total DWI score	0.904	0.877	0.939	0.9

151 ICC=intra-class correlation coefficient, MRI=magnetic resonance imaging. For definition of sub-score A, sub-score
 152 B and total DWI score, see Table S2.

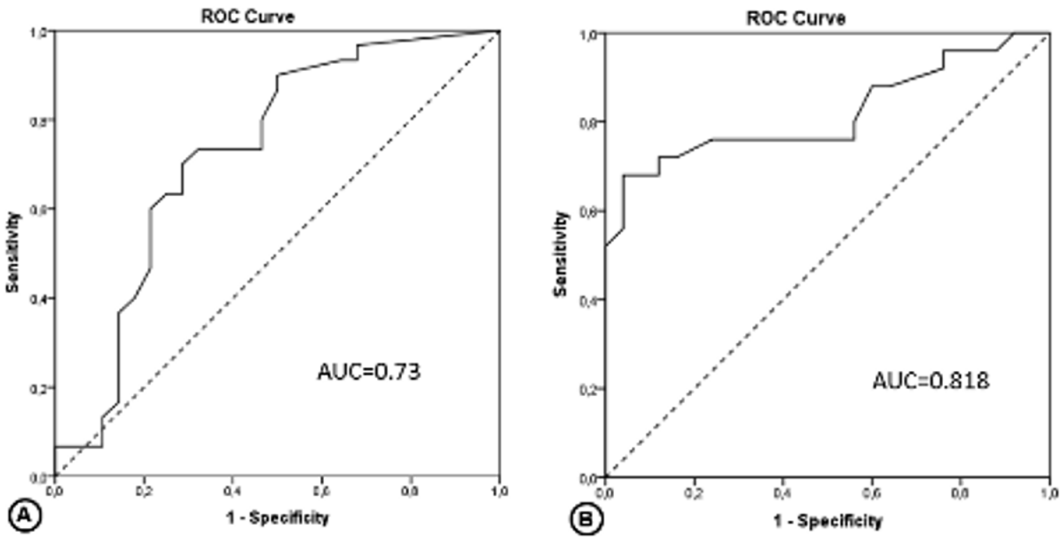
153



154

155 Figure S1. Changes in A) pulmonary exacerbation score (PEX score), B) forced expiratory volume in 1 second
 156 (FEV_1) and C) total diffusion-weighted imaging score (DWI score) between case (dotted lines) and control
 157 (continuous lines) groups. X-axis represents baseline (t_0) and follow-up (t_1) time points, while the y-axis of each plot
 158 represents unit of measure for each variable. Note that RTE group (dotted lines) has significant changes in PEX
 159 score, FEV_1 and DWI score, while the control group (continuous line) remains stable.

160



161

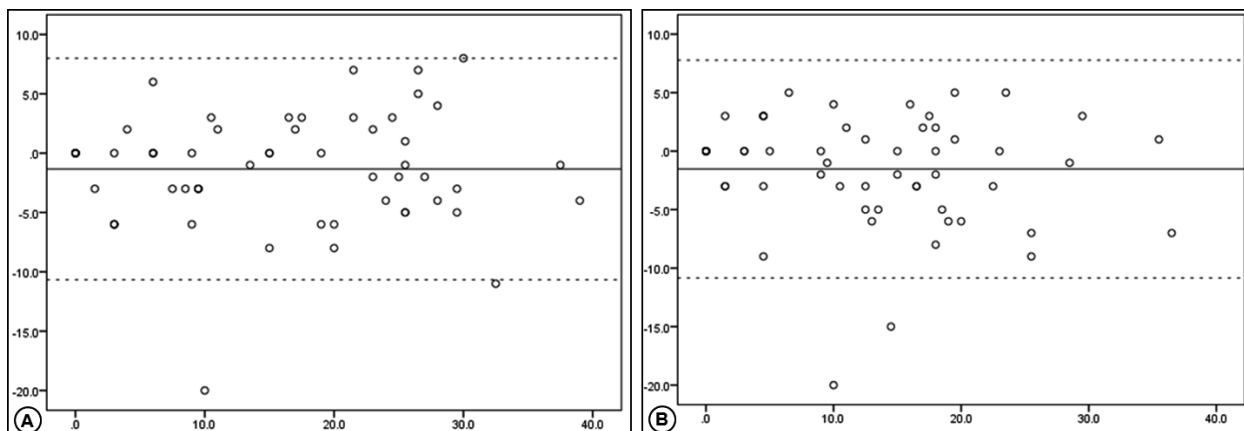
162 Figure S2. Receiver operating characteristic (ROC) curves for DWI score (A) and ADC (B). AUC values between
 163 0.90-1, 0.80-0.90, 0.70-0.80, 0.60-0.70 correspond to an excellent, good, fair and poor accuracy respectively¹⁶. Note
 164 higher diagnostic accuracy of ADC measurements than DWI score to differentiate patient with CF and respiratory
 165 tract exacerbation.

166

167

168

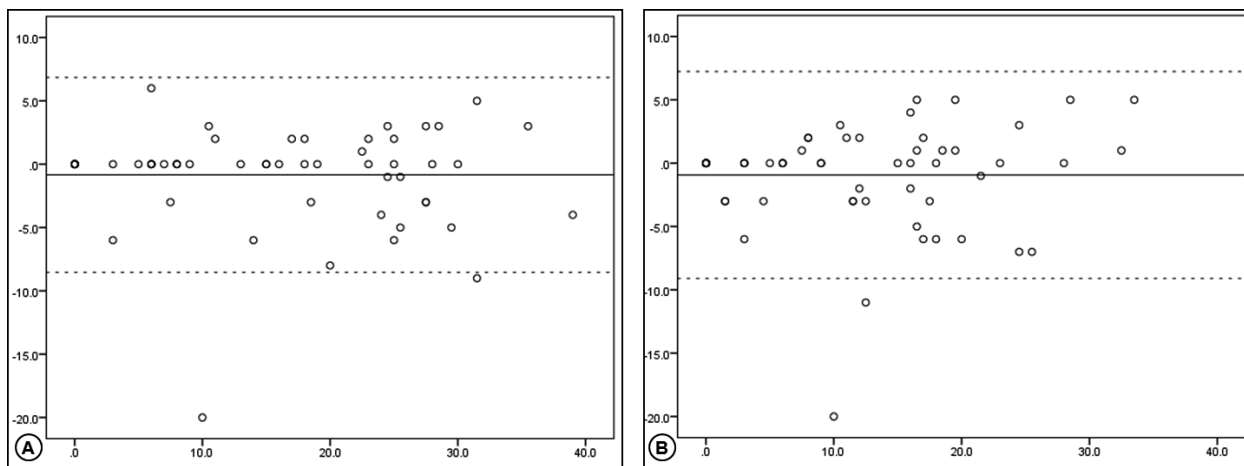
169



170

171 Figure S3. Inter-observer agreement for total DWI scores. Bland-Altman plot of inter-observer agreement (observer
172 1 versus observer 2) at A) baseline and B) follow-up MRI. Note that mean differences are close to zero and that all
173 observations are around the mean.

174



175

176 Figure S4. Intra-observer agreement for total DWI scores. Bland-Altman plot of intra-observer agreement (observer
177 1, one month time gap between scores) at A) baseline and B) follow-up MRI. Note that mean differences are close
178 to zero and that all observations are around the mean.

179

180 **References**

- 181 1 Bilton D, Canny G, Conway S, *et al.* Pulmonary exacerbation: Towards a definition for use in clinical trials.
182 Report from the EuroCareCF Working Group on outcome parameters in clinical trials. *J Cyst Fibros* 2011;
183 **10**: S79–81.
- 184 2 Rosenfeld M, Emerson J, Williams-Warren J, *et al.* Defining a pulmonary exacerbation in cystic fibrosis. *J*
185 *Pediatr* 2001; **139**: 359–65.
- 186 3 Laszlo G. Standardisation of lung function testing: helpful guidance from the ATS/ERS Task Force. *Thorax*
187 2006; **61**: 744–6.
- 188 4 Ciet P, Serra G, Bertolo S, *et al.* Assessment of CF lung disease using motion corrected PROPELLER MRI:
189 a comparison with CT. *Eur Radiol* 2015; **26**: 780–7.
- 190 5 Tepper L a., Ciet P, Caudri D, Quittner AL, Utens EMWJ, Tiddens H a. WM. Validating chest MRI to
191 detect and monitor cystic fibrosis lung disease in a pediatric cohort. *Pediatr Pulmonol* 2015; : n/a-n/a.
- 192 6 Qayyum A. Diffusion-weighted Imaging in the Abdomen and Pelvis: Concepts and Applications1.
193 *RadioGraphics* 2009; **29**: 1797–810.
- 194 7 Chavhan GB, Alsabban Z, Babyn PS. Diffusion-weighted Imaging in Pediatric Body MR Imaging:
195 Principles, Technique, and Emerging Applications. *Radiographics* 2014; **34**: E73-88.
- 196 8 Koh D, Collins DJ. Diffusion-Weighted MRI in the Body: Applications and Challenges in Oncology. *Am J*
197 *Roentgenol* 2007; **188**: 1622–35.
- 198 9 Uto T, Takehara Y, Nakamura Y, *et al.* Higher sensitivity and specificity for diffusion-weighted imaging of
199 malignant lung lesions without apparent diffusion coefficient quantification. *Radiology* 2009; **252**: 247–54.
- 200 10 Ciet P, Serra G, Andrinopoulou ER, *et al.* Diffusion weighted imaging in cystic fibrosis disease: beyond
201 morphological imaging. *Eur Radiol* 2016; published online Feb 12. DOI:10.1007/s00330-016-4248-z.
- 202 11 Liu H, Liu Y, Yu T, Ye N. Usefulness of diffusion-weighted MR imaging in the evaluation of pulmonary
203 lesions. *Eur Radiol* 2010; **20**: 807–15.
- 204 12 Tanaka R, Horikoshi H, Nakazato Y, *et al.* Magnetic resonance imaging in peripheral lung adenocarcinoma:
205 correlation with histopathologic features. *J Thorac Imaging* 2009; **24**: 4–9.
- 206 13 Le Bihan D, Breton E, Lallemand D, Aubin ML, Vignaud J, Laval-Jeantet M. Separation of diffusion and
207 perfusion in intravoxel incoherent motion MR imaging. *Radiology* 1988; **168**: 497–505.
- 208 14 Le Bihan D. Intravoxel incoherent motion perfusion MR imaging: a wake-up call. *Radiology* 2008; **249**:

- 209 748–52.
- 210 15 Attariwala R, Picker W. Whole body MRI: Improved lesion detection and characterization with diffusion
211 weighted techniques. *J Magn Reson Imaging* 2013; **38**: 253–68.
- 212 16 Pines, Jesse M.; Carpenter, Christopher R.; Raja, Ali S. ; Schuur JDS. Evidence-Based Emergency Care:
213 Diagnostic Testing and Clinical Decision Rules, 2nd Edition, 2nd Editio. Wiley.
- 214